Unraveling the Effect of Carbon Nanotube Oxidation on Solid-State Decomposition of Ammonia Borane/Carbon Nanotube Composites

THE JOURNAL OF PHYSICAL CHEMISTRY C
A JOURNAL OF THE AMERICAN CHEMICAL SOCIETY

pubs.acs.org/JPCC

Article

Unraveling the Effect of Carbon Nanotube Oxidation on Solid-State Decomposition of Ammonia Borane/Carbon Nanotube Composites

Mattia Bartoli,* Candido Fabrizio Pirri, and Sergio Bocchini

Cite This: *J. Phys. Chem. C* 2022, 126, 16587−16594

Read Online

ACCESS | Metrics & More | Article Recommendations | Supporting Information

ABSTRACT: Among the routes to perform hydrogen release from ammonia in solid state, the nanoconfinement into a carbonaceous matrix or the use of carbon-supported catalysts for the thermal degradation of ammonia borane (AB) is the most interesting one. Oxidized carbon nanotubes (CNTs) represent a suitable choice for preparing AB mixtures or for anchoring catalysts for dehydrogenation. Nevertheless, literature lacks detailed study about the influence of CNT oxidation degree on the AB degradation/hydrogen release. In this study, we first described in a comprehensive way that the thermal degradation of AB mixed with CNTs by varying the CNT oxidation degree enlightens the degradative routes mainly active in each case. Using highly oxidized CNTs, we observed a decrement of activation energy of the degradative process up to around 53% and the activation/suppression of different pathways based on the amount of oxygen functionalities present in the mixtures. Furthermore, the presence of oxidized CNTs modulated the solid-state reactivity of AB reducing the release of nitrogen/boron species together with hydrogen. These findings lead the way for the design of new hydrogen storage materials.

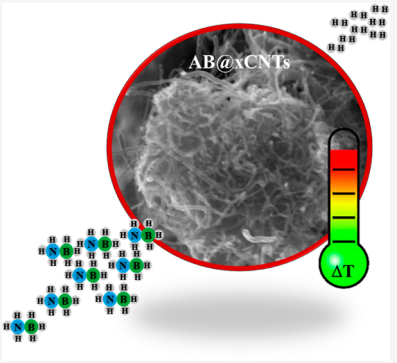

INTRODUCTION

The development of highly efficient materials for chemical hydrogen storage is one of the great challenges for driving the hydrogen economy to a major breakthrough.[1] The safety of hydrogen tanks and the energy required for compression to high pressure have drastically slowed down the spread of the hydrogen-based mobility.[2] Several alternatives have been proposed to overcome these problems using inorganic or organic carriers.[3,4] Among all the available species, ammonia borane (AB) is one of the most interesting compounds with a theoretical gravimetric hydrogen storage capacity (GHSC) of up to 19.6 wt %.[5,6] The most challenging and attractive AB dehydrogenation route is the solid-state thermal-induced dehydrogenation.[7] Nevertheless, this reaction is complex, involves several pathways[8] and mechanisms that could be promoted or suppressed by the presence of additives.[9] The solid-state dehydrogenation kinetic of AB under thermal stimuli is widely investigated by directly mixing AB with dehydrogenation catalysts[10] or by confinement into a porous matrix.[11] The confinement is a very practical route to tune the decomposition mechanisms and rates but generally leads to a decrease of GHSC. A well-established practice is the nanoconfinement of AB into carbonaceous matrix as reported by Sepehri et al.[12] They embedded AB into carbon cryogel showing an appreciable decrement of the dehydrogenation process activation energy; it was correlated with the pore size distribution. Sepehri et al. also suggested a close relationship between the surface texturing of carbon cryogels and dehydrogenation performances.[13] On this very same topic, Moussa et al.[14] described dehydrogenation mechanism based on the formation of borane esters on the carboxylic function on the activated carbon surface. Nonetheless, it is very hard to rationalize the effect of surface texture, porosity, and specific surface area due to their codependence.

Among carbon matrices, carbon nanotubes (CNTs) represent a good benchmark for testing the effect of the single surface texturing. Sun et al.[15] first reported a density functional theory study on the AB dissociation on the inner and outer surface of a single-wall CNT, while Zhang et al.[16] proved the beneficial effect of nitrogen doping on CNTs for the hydrogen release from AB. Nevertheless, the far more used CNT modification process to improve its performances on AB destabilization or as dehydrogenation catalyst support is the oxidation with insertion of oxygen-based functionalities.[17] Accordingly, in this work, we evaluated the effect of CNT oxidation degree on the AB destabilization in solid state under thermal stimuli. The CNT surface was preliminary annealed in order to reduce the defectiveless carbon surface prior to the oxidative treatment. By the combination of several investigative techniques, a comprehensive insight on the effect and mechanism of AB degradation on oxidized CNT bundles was provided. Data collected proved the positive effect of

Received: July 5, 2022
Revised: September 6, 2022
Published: September 23, 2022

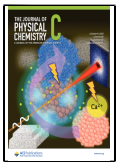

oxidized CNTs in the modulation of concurrent AB degradative pathways involving the releasing of $N_xB_yH_z$.

METHODS

Multi-walled CNTs (NC7000TM, produced via the catalytic chemical vapor deposition process) were purchased from Nanocyl SA (Sambreville, Belgium). Carbon purity: 90%; surface area: 250−300 m^2/g, as indicated in the datasheet provided by the supplier. Ammonium sulfate (>98%), sodium borohydride (>99%), tetrahydrofuran (THF) (>98), sulfuric acid (98%), and nitric acid (63%) were purchased from Sigma-Aldrich and used without any further purifications.

AB was synthesized and purified as reported by Ramachandran and Gagare.[18] To remove impurities providing a homogeneous benchmark for the further oxidative modifications, a preliminary oxidative process was performed; CNTs were thermally annealed at 1600 °C for 1 h in an inert atmosphere.[19]

Oxidation of CNTs was run according to the procedure reported by Lavagna et al.[20] 200 mg of CNTs was suspended in 15 mL of the solution of sulfuric acid and nitric acid (ratio 3:1 V/V) and sonicated in an ultrasound bath at 60 °C for different times. The resulting suspension was diluted with deionized water and filtered. The solid recovered was washed several times with deionized water and dried at 50 °C in vacuum for 16 h.

The samples *x*CNTs are named according to the oxidation times *x* (0, 15, 30, and 60 min) as reported in Table 1

Table 1. Sample Labeling

samples label	oxidation time (min)
0CNTs	0
15CNTs	15
30CNTs	30
60CNTs	60

Composites of AB and *x*CNTs (AB@*x*CNTs) were produced by suspending AB in THF at room temperature and *x*CNTs with a weight ratio of *x*CNTs/AB of 0.1 and 1. The solvent was removed by evaporation in rotavapor. The solids were recovered and dried at 20 °C under vacuum until constant weight was achieved.

Raman spectra were collected using a Renishaw inVia (H43662 model, Gloucestershire, UK) equipped with a green laser line (514 nm) with a 50× objective. Raman spectra were recorded in the range from 500 to 4000 cm^{-1}. Signals were fitted according to methodology proposed by Tagliaferro et al.[21]

The surface functionalities were investigated by using X-ray photoelectron spectroscopy (XPS). To this aim, a PHI 5000 VersaProbe Physical Electronics (Chanhassen, MN, USA) scanning X-ray photoelectron spectrometer (monochromatic Al K-alpha X-ray source with 1486.6 eV energy, 15 kV voltage, and 1 mA anode current) was employed for evaluating the surface chemical composition. *x*CNTs and AB@*x*CNTs were analyzed through Fourier transform infrared (FT-IR) (ATR mode) spectroscopy using a TENSOR II spectrometer (Bruker) equipped with a ATR module Platinum II (Bruker).

The morphology of AB@*x*CNTs was investigated using field-emission scanning electron microscopy (FE-SEM) Zeis SupraTM 25 (Oberkochen, Germany). Energy-dispersive X-ray (EDX, Oxford Inca Energy 450) analysis was used to study the elements present in samples.

Stability of *x*CNT materials was investigated through thermogravimetric analysis (TGA) using Netzsch TG 209F1 Libra in N_2 flux (20 mL/min) with a temperature ramp of 10 °C/min from 30 to 900 °C connected with an IR module TENSOR II spectrometer (Bruker) with an interface temperature of 200 °C.

TGA-coupled IR (TGA-IR) absorption analyses were carried out in a Thermo-gravimetric Analyzer NETZSCH TG 209 F1 coupled by a transfer line heated at 230 °C with an IR Bruker TENSOR II equipped with an IR gas cell heated at 200 °C. The tests were performed by heating from 30 to 350 °C with a rate of 10 °C min^{-1} for about 3 mg of the sample in alumina pans under a nitrogen flux of 40 mL min^{-1}. Experimental weight error is between ±1%. The FT-IR analysis was done in the absorbance mode in the range of 650−4000 cm^{-1}.

Activation energy of the dehydrogenation process of AB was calculated by using the Kissinger equation[22] using differential scanning calorimetry (DSC) analyses using a Netzsch DSC 204 F1. Analyses were carried out under dry N_2 gas (70 mL/min) using samples of around 3 mg in sealed aluminum pans using heating rates of 2, 5, and 10 °C/min.

RESULTS AND DISCUSSION

Table 2 reports the preliminary characterizations of *x*CNTs performed through XPS (Supporting Information, Figures S1 and S2) and Raman spectroscopy.

Table 2. Main Features of *x*CNTs Observed through XPS and Raman Spectroscopic Analysis

	elemental composition[a] (wt %)		chemical functionalities (atomic fraction %)[b]			
sample	C	O	C−O	C=O	COOH	I_D/I_G[c]
0CNTs	97.7	2.2	72	28	0	0.5
15CNTs	94.4	5.6	48	52	0	0.6
30CNTs	93.9	6.1	51	49	0	0.7
60CNTs	92.6	7.4	63	27	10	0.8

[a]Calculated by the EDX analysis. [b]Calculated on the fitting O 1s (Supporting Information, Figure S2). [c]Calculated by fitting the Raman spectra (Supporting Information, Figure S3) according to the methods described by Tagliaferro et al.[21]

0CNT showed a very low concentration of oxygen up to 2.3 wt % and few traces of iron (<0.1 wt %). According to the specification provided by the supplier, the thermal annealing at 1600 °C removed a great part of the oxygen functionalities that are still present as hydroxyl (72%, 532.4 eV) and carbonyl (28%, 533.7 eV) mainly due to surface air oxidation. The oxidation process increased the oxygen percentage up to 5.6 wt % after 1 h with an appreciable change also in oxygen-containing species distribution. Moving from 15CNTs and 30CNTs, we observed an increment of the amount of hydroxyl functionalities from 48 up to 52% and a decrement of carbonyl functions with increment of oxidation time up to 49% after 30 min. 60CNTs showed a greater hydroxyl percentage of up to 63% and a lower carbonyl amount of up to 27% together with 10% or carboxylic functionalities (534.6 eV).

A further insight on the effect of the oxidation process on CNTs was provided by Raman spectra (Supported Informa-

https://doi.org/10.1021/acs.jpcc.2c04693
J. Phys. Chem. C 2022, 126, 16587−16594

tion, Figure S3). Raman spectroscopy is a very powerful tool to evaluate the quality and defectiveness of carbon materials as reported by many authors[23,24] mainly using the ratio between the intensity of D (I_D) and G (I_G) peak area as a measure of system disorder. The evaluation of peak area is quite complex and could be ran by using different line shapes, and in this work, we used a GauLor line shape as defined by Tagliaferro and coworkers[21] allowing to minimize the components for each peak.

According to the Raman spectra outputs, the *x*CNTs underwent a massive disorganization of aromatic systems increasing increment of the I_D/I_G ratio from 0.5 for 0CNTs up to 0.8 for 60CNTs, as summarized in Table 2.

The functionalization of *x*CNTs was also proved by the FT-IR (ATR mode) spectra shown in Figure 1.

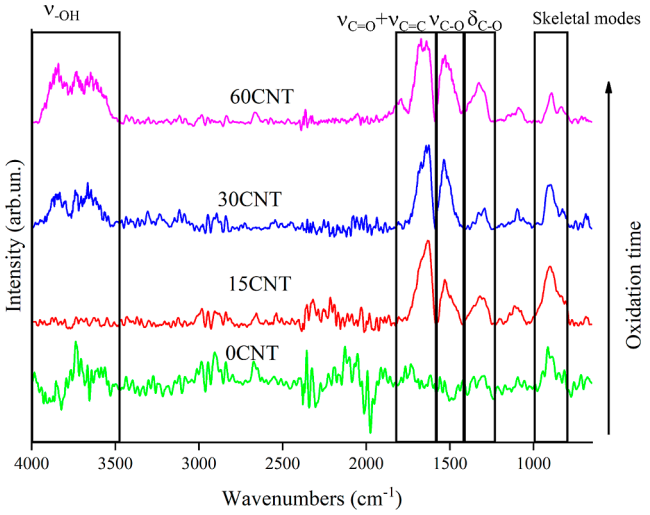

Figure 1. FT-IR (ATR mode) spectra of *x*CNTs in the range from 500 up to 4000 cm^{-1} with squared the ranges of ν_{OH}, $\nu_{C=O}$, ν_{C-O}, δ_{C-O}, and the skeletal modes.

FT-IR spectra of 0CNTs did not show any appreciable signal in good agreement with the high percentage of carbon and the poor amount of oxygen reported in Table 2. After oxidation, 15CNTs showed the presence of oxygen-based functions with the rising of $\nu_{C=O}$ at around 1700−1713 cm^{-1}, reasonable due to carbonyl species. By increasing the oxidation time up to 30 and 60 min, the IR spectra showed several intense bands due to the presence of ν_{OH} from 3000 to 3500 cm^{-1} and an appreciable increment of the intensity of ν_{C-O} (1520 cm^{-1}) and δ_{C-O} (1325 cm^{-1}) in good agreement with the increment of oxygen content.

The functionalization of CNTs was particularly appreciable by considering the TGA analysis (Supporting Information, Figure S4) summarized in Table 3.

0CNTs did not show any appreciable thermal degradation up to 855 °C when residual doping oxygen sites were degraded leading to a residual mass of up to 98.95% in good agreement with the oxygen detected through XPS. The increment of the oxidation time induced a modification of the TGA profile showing an increment of mass loss with different steps due to the degradation of hydroxyl (T_{max1}) and carbonyl functions (T_{max2}).[25] According to the residue observed at 900 °C, oxygen insertion reached up to 10.43 wt % for 60CNTs supporting a direct correlation between CNT modification and oxidation time.

The oxidation process also affected the morphology of both *x*CNTs and AB@CNTs, as shown in Figure 2.

As shown in Figure 2a,d,g, the morphology of CNTs was not deeply affected for oxidation time up to 30 min. As reported in Figure 2j, 60CNTs showed an increment of average diameter and partial alignment of CNT bundles. As shown in Figure 2b,c,e,f,h,i,k,l, the addition of AB promoted a permeation of CNT bundles with the formation of highly dispersed CNTs into an AB matrix. This was not observed from AB@30CNTs and AB@60CNTs with an AB/*x*CNT ratio of 1, as shown in Figure 2k. This was reasonably due to the presence of carboxylic functions that rapidly reacted with AB forming borane ester polymeric structures on the surface of the CNT bundles avoiding the full permeation of the bundles.

The presence of AB was also confirmed by the analysis of FT-IR spectra of AB@*x*CNTs (Supporting Information, Figure S5). All AB@*x*CNT spectra show the FT-IR signature of AB with symmetric ν_{NH} at 3229 cm^{-1}, symmetric ν_{BH} ranging from 2473 to 2158 cm^{-1}, δ_{NH} at 1609 cm^{-1}, and ν_{BN} at 1364 cm^{-1}.[26] A small band at around 1252 cm^{-1} was detected in the IR spectra of AB@*x*CNTs reasonably due to ν_{B-O} supporting the formation of borates through a rapid reaction with oxygen residue on the surface of *x*CNTs.

A preliminary assessment of the effect of CNT oxidation degree was run by using DSC analysis and Kissinger equation[27] reported as follows

$$\ln\left(\frac{HR}{T_p^2}\right) = \frac{-E_a}{RT_p} + \ln\left(\frac{Z}{RE_a}\right) \quad (1)$$

where T_p is the peak temperature, HR is the heating rate, E_a is the activation energy of the AB dehydrogenation process, Z is a kinetic constant, and R is the ideal gas constant. Activation energy of dehydrogenation was evaluated by plotting $\ln(\alpha/T_p^2)$ versus $1/T_p$ and applying a linear fit (Supporting Information, Figure S6), as summarized in Table 4.

As reported in Table 4, AB showed an E_a of up to 160 kJ mol^{-1} in good agreement with data reported in the literature by Gutowska et al.[28] (up to 161 kJ mol^{-1}). AB@0CNTs showed a decrement of E_a down to 85 and 95 kJ mol^{-1} for 0CNT/AB ratios of 0.1 and 1, respectively. The decrements were reasonably due to the destabilization of the N−B bond from the interaction with 0CNT π−orbital systems as reported by Sun et al.[15] The 10 kJ mol^{-1} difference observed was due to a better permeation of the CNT bundle for a high ratio of AB/

Table 3. TGA Outputs of *x*CNTs in a N_2 Atmosphere in the Range from 30 up to 900 °C

sample	T_{onset} (°C)	T_{max1} (°C)	residue@T_{max1} (%)	T_{max2} (°C)	residue@T_{max2} (%)	residue@900 °C (%)
0CNTs	855					98.95
15CNTs	101	124	98.64	204	97.63	95.34
30CNTs	103	137	97.96	193	97.41	94.44
60CNTs	120	155	98.06	185	94.07	89.57

https://doi.org/10.1021/acs.jpcc.2c04693
J. Phys. Chem. C 2022, 126, 16587−16594

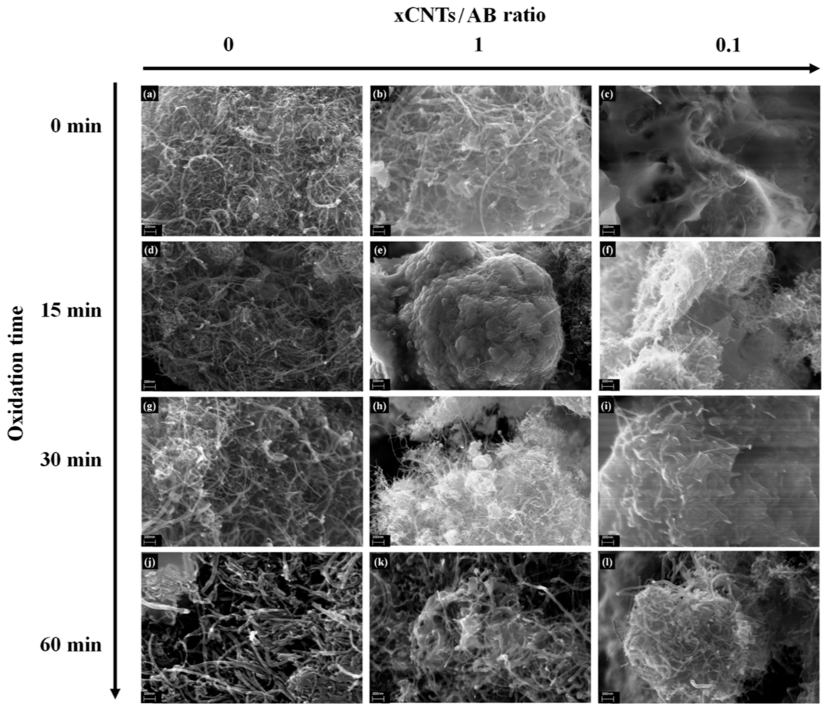

Figure 2. FE-SEM captures of (a) 0CNTs, (b) AB@0CNTs (0CNT/AB ratio of 1), (c) AB@0CNTS (0CNT/AB ratio 0.1), (d) 15CNTs, (e) AB@15CNTs (15CNT/AB ratio of 1), (f) AB@15CNTS (15CNTs/AB 0.1), (g) 30CNTs, (h) AB@30CNTs (30CNT/AB ratio of 1), (i) AB@30CNTS (30CNTs/AB 0.1), (j) 60CNTs, (k) AB@60CNTs (60CNT/AB ratio of 1), and (l) AB@60CNTS (60CNTs/AB 0.1).

Table 4. Activation Energies Calculated from Kissinger's Plot for AB@*x*CNTs (*x*CNT/AB Ratios of 0, 0.1, and 1)

CNT/AB ratio	oxidation time (min)	activation energy (kJ mol^{-1})
0		161
0.1	0	85
	15	96
	30	102
	60	107
1	0	95
	15	127
	30	115
	60	85

0CNTs that magnify the AB-0CNT interactions. The contribution of oxygen functionalities was negligible considering the very low amount of oxygen present in the annealed CNTs.

The oxygen content played a crucial role considering that AB@15CNTs showed an increment of activation energy of up to 96 and 127 kJ mol^{-1} for AB/15CNT ratios of 0.1 and 1, respectively. Interestingly, the increment of oxidation time led to an increment of the E_a for an AB/*x*CNT ratio of 0.1 up to 107 kJ mol^{-1}, while it increased up to 127 kJ mol^{-1} using 15CNTs and decreased down to 85 kJ mol^{-1} using 60CNTs and an AB/*x*CNT ratio of 1. The trends of E_a together with the different slopes of Kissinger's plot (Supporting Information, Figure S6) suggested that the thermal decomposition of AB in the presence of oxidized CNTs is quite complex and involved several steps as described more in detail in the following sections.

The thermal degradative processes of AB and AB-containing materials are generally investigated through TGA in order to monitor the weight losses[29] and the products formed by coupling a detector such as mass[30] or IR[31] spectrometers. Nevertheless, TGA analysis of AB is very sensitive to the operative conditions such as carrier gas and crucible filling level.[32] Accordingly, the same amount of materials for each TGA-IR experiment (TGA curves are included in Supporting Information, Figure S7) of up to around 4 mg in a nitrogen atmosphere collecting the data shown in Figure 3 and summarized in Table 5 was used.

All materials showed a two-stage degradative step at temperature close to 100 and 150−160 °C, respectively, that are composed by several reactions occurring simultaneously, as shown by the FT-IR spectra collected during the TGA analysis.

According to Figure 3a and TGA curves (Supporting Information, Figure S7), AB releases pure H_2 till 31 °C with a mass loss of up to 0.23 wt %. At higher temperatures, IR spectra show the presence of ammonia (ν_{NH} 965 and 930 cm^{-1})[33] and diborane (τ_{HBH} 2584−2523 cm^{-1}, ν_{BH} 2361−2329 cm^{-1}, and δ_{BH} 1387 cm^{-1})[34] suggesting a chemical pathway involving the degradation of the N−B bond. Up to a temperature of 86 °C, two bands rise up to around 1392 and 1334 cm^{-1} due to the ν_{BN} of NH_2BH_2 as reported by Gerry et al.[26] By increasing the temperature up to 100 °C, borazine is formed as confirmed by the presence of 1470−1460 and 2741−2396 cm^{-1} bands as reported by Kaldor and Porter[35] reaching a maximum at 162 °C. The residue at 35 °C is 48.0 wt %. On the contrary to pure AB, AB@0CNT and a CNT/AB ratio of 0.1 (Figure 3b) show the release of ammonia at 77 °C, but a higher release of pure H_2 of up to 0.9 wt % was observed with a massive formation of diborane. Interestingly, borazine is observed since a temperature of 100 °C reaching a maximum at 154 °C. The residue at 350 °C is of 51.4 wt %. Using AB@0CNT and a CNT/AB ratio of 1 (Figure 3c), release of pure H_2 was considerably lower reaching up to around 0.4 wt % forming ammonia at 67 °C suggesting a greater destabilization of N−B bonds. At 100 °C, AB@0CNT with a CNT/AB ratio

https://doi.org/10.1021/acs.jpcc.2c04693
J. Phys. Chem. C 2022, 126, 16587−16594

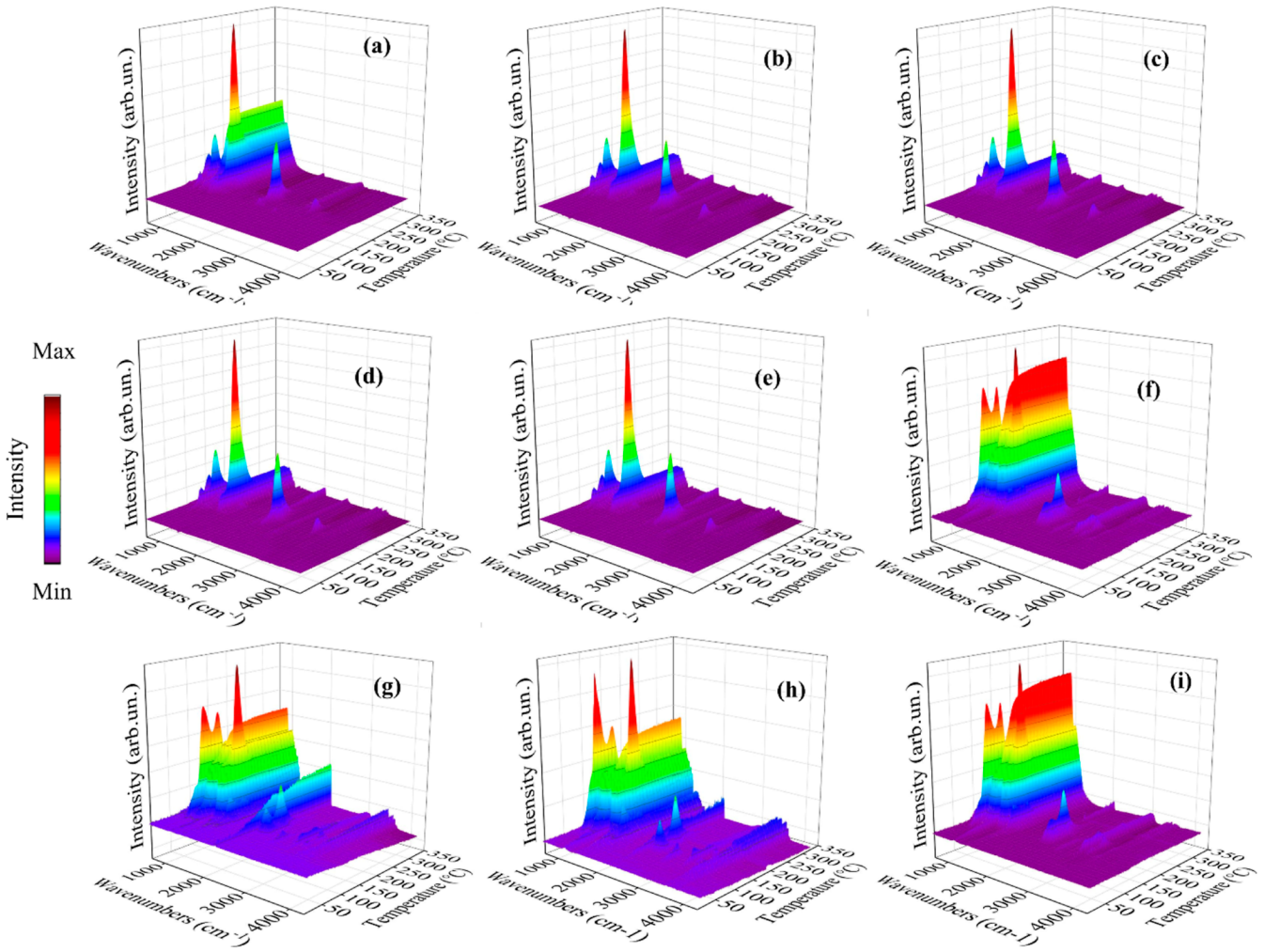

Figure 3. IR spectra collected during the TGA-IR analysis of (a) AB, (b) AB@0CNTs (0CNT/AB ratio of 0.1), (c) AB@15CNTs (15CNT/AB ratio of 0.1), (d) AB@30CNTs (30CNT/AB ratio of 0.1), (e) AB@60CNTs (60CNT/AB ratio of 0.1), (f) AB@0CNTs (0CNT/AB ratio of 1), (g) AB@15CNTs (15CNT/AB ratio of 1), (h) AB@30CNTs (30CNT/AB ratio of 1), and (i) AB@60CNTs (60CNT/AB ratio of 1).

Table 5. TGA Analysis of AB*x*CNTs (CNT/AB Ratios of 0, 0.1, and 1) in a N_2 Atmosphere in the Range from 30 up to 350 °C

CNTs/AB ratio	oxidation time (min)	T_{onset} (°C)	T_{max1} (°C)	residue@T_{max1} (%)	T_{max2} (°C)	residue@T_{max2} (%)	residue@350 °C (%)	H_2 solo production (wt %)[a]
0		105	106	93.4	162	75.1	48	0.23
0.1	0	97	107	93.7	154	58.9	51	0.91
	15	93	106	93.6	157	60.8	53	0.31
	30	99	109	93.7	148	61.2	54	0.22
	60	97	108	93.6	147	63.2	55	0.15
1	0	95	109	93.5	150	79.4	74	0.40
	15	96	112	91.7	156	81.3	80	0.22
	30	99	108	92.2	152	82.9	75	0.16
	60	96	107	93.7	147	79.6	73	0.59

[a]Calculated as follows (mass loss of AB@*x*CNTs prior to the release of any IR-detectable compound) − (mass loss of *x*CNTs).

of 1 released diborane and borazine in the range from 111 to 205 °C and 1470−1460 cm^{-1} bands disappeared releasing polymeric species such as NH_x−BH_x with various dehydrogenation degrees. AB@15CNT and a CNT/AB ratio of 0.1 (Figure 3d) released ammonia from 64 to 260 °C with a pure H_2 release of up to 0.31 wt.% and borazine production from 106 °C. AB@15CNT with a CNT/AB ratio of 0.1 (Figure 3e) leads to massive formation of ammonia and diborane through a mechanism as the one described by Al-Kukhun et al.[8] for solid-state AB thermal degradation till 111 °C when borazine was started to be released.

The same trend and mechanisms are observed for AB@30CNT and AB@60CNT suggesting a preferential release of borazine for high AB loading. Furthermore, the release of pure hydrogen occurring in the early stage of the thermal degradation followed the E_a showing a maximum for AB@60CNT with a CNT/AB ratio of 0.1 reaching up to 0.59 wt %. The dehydrogenative polymerization occurring in the early

https://doi.org/10.1021/acs.jpcc.2c04693
J. Phys. Chem. C 2022, 126, 16587−16594

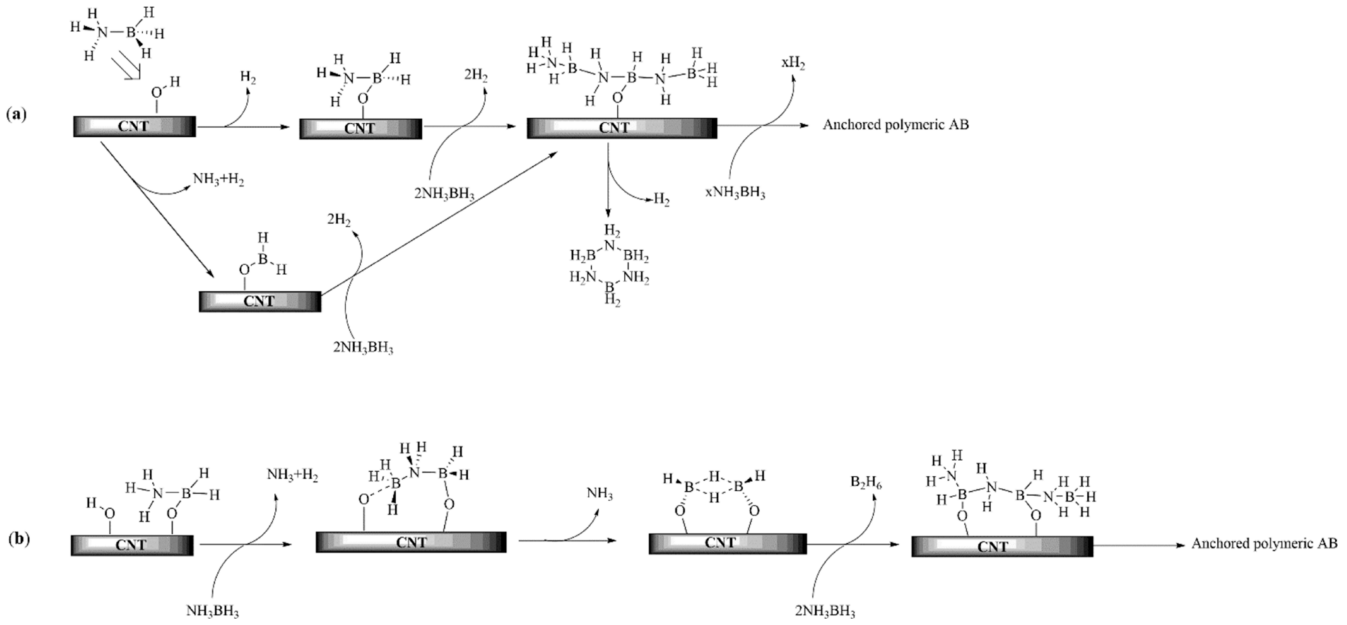

Figure 4. Different AB degradative pathways in the presence of (a) a poor and (b) rich oxygen functionality environment.

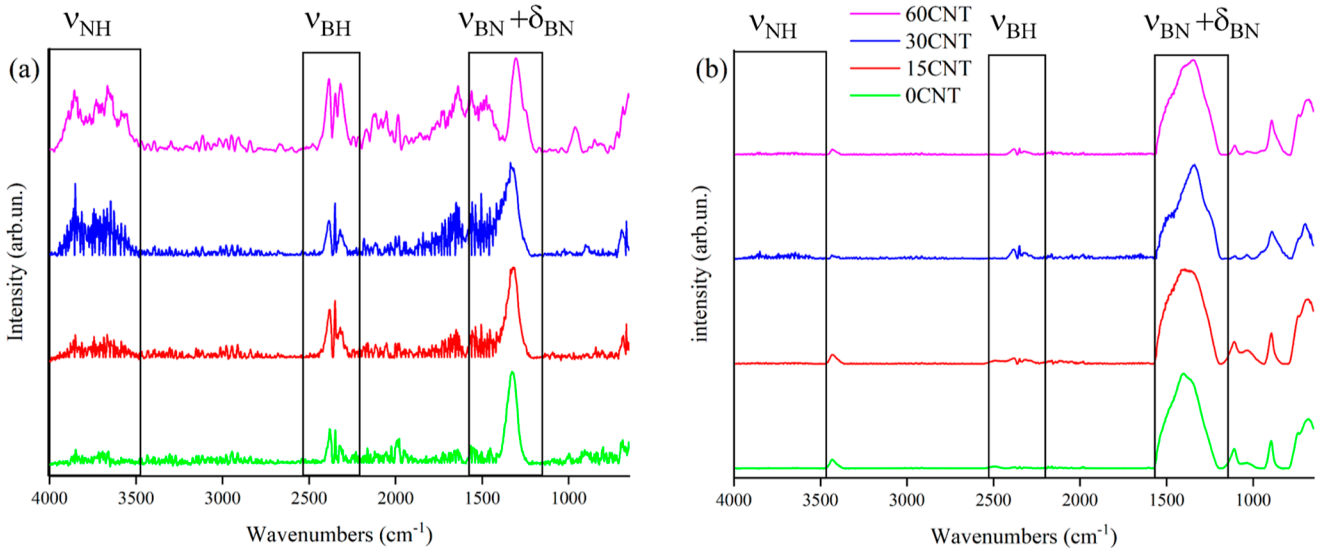

Figure 5. FT-IR spectra collected after the TGA-IR analysis of (a) AB@*x*CNTs (*x*CNT/AB ratio of 0.1) and AB@*x*CNTs (*x*CNT/AB ratio of 1).

stage of thermal degradation of AB was the degradative route most affected by the E_a, while the further degradative routes were related with several parameters such as *x*CNT/AB ratio and *x*CNTs oxidation time. This process led to the release of hydrogen and formation of linear species covalently bonded that could further evolve through very complex pathways. Accordingly, the low concentration of diborane species for a CNT/AB ratio of 0.1 suggests that low concentration of oxygen functionalities promoted different degradative pathways such as those reported in Figure 4.

As shown in Figure 4a, we hypothesized a first reaction between boron- and oxygen-based functionalities and with the formation of B−O bonds with the release of ammonia and hydrogen similar to the reactivity discussed by Li et al.[36] in the presence of lithium-based catalysts. Similar reactivity was confirmed in the presence of carboxylic functionalities as described by Li et al.[37] Weak anchored materials could evolve through cyclic species that rapidly converted releasing borazine and hydrogen. The increment of oxygen-based functions leads to the formation of anchored diborane species with their release and formation of well-anchored AB polymeric species, as shown in Figure 4b. The increment of oxygen could lead to a different mechanism as proved by FT-IR analysis of the residues recovered after the thermal degradative process reported in Figure 5.

As shown in Figure 5a, AB@*x*CNTs with a *x*CNT/AB ratio of 0.1 showed the persistence of the ν_{BH}. In a *x*CNTs/AB ratio of 1 (Figure 5b) ν_{BH} is not observed that showed a broader envelope of bands between 1540 and 1200 cm^{-1}. The difference between spectra reported in Figure 5a,b suggested that the well-anchored species formed using a *x*CNT/AB ratio of 1 led to highly dehydrogenated materials with N−B covalent bonds, while the greater release of borazine using a *x*CNT/AB ratio of 0.1 reduced the dehydrogenative polymerization of AB products. This was confirmed from the increment of residue after the thermal treatment up to 350 °C observed in Table 5

https://doi.org/10.1021/acs.jpcc.2c04693
J. Phys. Chem. C 2022, 126, 16587−16594

where the residue of a *x*CNT/AB ratio of 1 was ranging from 73.4 up to 79.6 wt % while the *x*CNT/AB ratio of 0.1 ranged from 51.4 up to 54.7 wt %. Accordingly, the retention of dehydrogenated anchored species will provide a relevant advancement for the regeneration of these AB@*x*CNTs species reducing the mass loss due to the volatilization of $N_xB_yH_z$.

CONCLUSIONS

Confinement into carbon materials is a well-established practice to provide a reliable tool for the thermal degradation of AB. This study faced the effect of oxidation degree of the CNT bundle on thermal destabilization of AB. As clearly emerged, the main effect of the oxidation degree was the variation of the E_a affecting the early stages of the dehydrogenation for all *x*CNT/AB ratios. Furthermore, the concentration on oxygen-derived functions in the AB-containing materials plays a greater role in selecting the chemical degradative pathway compared to the CNT functionalization degree wt %.

This work first proposes a systematic study on the effect of the oxidative process on the interaction between CNTs and AB leading the way for the optimization of CNT-supported catalyst for the dehydrogenation/regeneration of AB-containing materials. The production of a library of AB@*x*CNT species allowed to identify materials that are able to retain partially dehydrogenated species reducing the mass loss due to the suppression of $N_xB_yH_z$ release during thermal degradation. These materials could be rehydrogenated enhancing their lifespan leading the way for new developments in hydrogen storage systems.

ASSOCIATED CONTENT

Supporting Information

The Supporting Information is available free of charge at https://pubs.acs.org/doi/10.1021/acs.jpcc.2c04693.

Spectra (XPS and Raman) of the *x*CNTs and AB@*x*CNTs, TGA of *x*CNTs, and Kissinger's plot (PDF)

AUTHOR INFORMATION

Corresponding Author

Mattia Bartoli − *Center for Sustainable Future Technologies (CSFT), Istituto Italiano di Tecnologia (IIT), 10144 Torino, Italy; Consorzio Interuniversitario Nazionale per la Scienza e Tecnologia dei Materiali (INSTM), 50121 Florence, Italy;* orcid.org/0000-0002-4678-0212; Phone: +39 0110904326; Email: mattia.bartoli@iit.it

Authors

Candido Fabrizio Pirri − *Center for Sustainable Future Technologies (CSFT), Istituto Italiano di Tecnologia (IIT), 10144 Torino, Italy; Department of Applied Science and Technology, Politecnico di Torino, 10129 Torino, Italy*

Sergio Bocchini − *Center for Sustainable Future Technologies (CSFT), Istituto Italiano di Tecnologia (IIT), 10144 Torino, Italy;* orcid.org/0000-0003-2876-2317

Complete contact information is available at: https://pubs.acs.org/10.1021/acs.jpcc.2c04693

Notes

The authors declare no competing financial interest.

ACKNOWLEDGMENTS

Authors wish to thank Ministero dello Sviluppo Economico (MISE) and Ministero della Transizione Ecologica (MITE) for the financial support.

REFERENCES

(1) Tarhan, C.; Çil, M. A. A Study on Hydrogen, the Clean Energy of the Future: Hydrogen Storage Methods. *J. Energy Storage* **2021**, *40*, 102676.

(2) Ravi, S. S.; Aziz, M. Clean Hydrogen for Mobility−Quo Vadis? *Int. J. Hydrogen Energy* **2022**, *47*, 20632.

(3) Sakintuna, B.; Lamaridarkrim, F.; Hirscher, M. Metal hydride materials for solid hydrogen storage: A review☆. *Int. J. Hydrogen Energy* **2007**, *32*, 1121−1140.

(4) Ren, J.; Musyoka, N. M.; Langmi, H. W.; Mathe, M.; Liao, S. Current Research Trends and Perspectives on Materials-Based Hydrogen Storage Solutions: A Critical Review. *Int. J. Hydrogen Energy* **2017**, *42*, 289−311.

(5) Demirci, U. B. Ammonia Borane, a Material with Exceptional Properties for Chemical Hydrogen Storage. *Int. J. Hydrogen Energy* **2017**, *42*, 9978−10013.

(6) Bowden, M.; Autrey, T.; Brown, I.; Ryan, M. The Thermal Decomposition of Ammonia Borane: A Potential Hydrogen Storage Material. *Curr. Appl. Phys.* **2008**, *8*, 498−500.

(7) Hu, M.; Geanangel, R.; Wendlandt, W. The Thermal Decomposition of Ammonia Borane. *Thermochim. Acta* **1978**, *23*, 249−255.

(8) Al-Kukhun, A.; Hwang, H. T.; Varma, A. Mechanistic Studies of Ammonia Borane Dehydrogenation. *Int. J. Hydrogen Energy* **2013**, *38*, 169−179.

(9) Heldebrant, D. J.; Karkamkar, A.; Hess, N. J.; Bowden, M.; Rassat, S.; Zheng, F.; Rappe, K.; Autrey, T. The Effects of Chemical Additives on the Induction Phase in Solid-State Thermal Decomposition of Ammonia Borane. *Chem. Mater.* **2008**, *20*, 5332−5336.

(10) Liu, M.; Zhou, L.; Luo, X.; Wan, C.; Xu, L. Recent Advances in Noble Metal Catalysts for Hydrogen Production from Ammonia Borane. *Catalysts* **2020**, *10*, 788.

(11) Wahab, M. A.; Zhao, H.; Yao, X. D. Nano-Confined Ammonia Borane for Chemical Hydrogen Storage. *Front. Chem. Sci. Eng.* **2012**, *6*, 27−33.

(12) Sepehri, S.; Garcia, B. B.; Cao, G. Tuning dehydrogenation temperature of carbon-ammonia borane nanocomposites. *J. Mater. Chem.* **2008**, *18*, 4034−4037.

(13) Sepehri, S.; García, B. B.; Cao, G. Influence of Surface Chemistry on Dehydrogenation in Carbon Cryogel Ammonia Borane Nanocomposites. *Eur. J. Inorg. Chem.* **2009**, 599−603.

(14) Moussa, G.; Bernard, S.; Demirci, U. B.; Chiriac, R.; Miele, P. Room-Temperature Hydrogen Release from Activated Carbon-Confined Ammonia Borane. *Int. J. Hydrogen Energy* **2012**, *37*, 13437−13445.

(15) Sun, C.; Du, A.; Yao, X.; Smith, S. C. Adsorption and Dissociation of Ammonia Borane Outside and inside Single-Walled Carbon Nanotubes: A Density Functional Theory Study. *J. Phys. Chem. C* **2011**, *115*, 12580−12585.

(16) Zhang, L.; Xia, G.; Ge, Y.; Wang, C.; Guo, Z.; Li, X.; Yu, X. Ammonia Borane Confined by Nitrogen-Containing Carbon Nanotubes: Enhanced Dehydrogenation Properties Originating from Synergetic Catalysis and Nanoconfinement. *J. Mater. Chem. A* **2015**, *3*, 20494−20499.

(17) Günbatar, S.; Aygun, A.; Karataş, Y.; Gülcan, M.; Şen, F. Carbon-Nanotube-Based Rhodium Nanoparticles as Highly-Active Catalyst for Hydrolytic Dehydrogenation of Dimethylamineborane at Room Temperature. *J. Colloid Interface Sci.* **2018**, *530*, 321−327.

(18) Ramachandran, P. V.; Gagare, P. D. Preparation of Ammonia Borane in High Yield and Purity, Methanolysis, and Regeneration. *Inorg. Chem.* **2007**, *46*, 7810−7817.

(19) Andrews, R.; Jacques, D.; Qian, D.; Dickey, E. C. Purification and Structural Annealing of Multiwalled Carbon Nanotubes at Graphitization Temperatures. *Carbon* **2001**, *39*, 1681−1687.
(20) Lavagna, L.; Bartoli, M.; Suarez-Riera, D.; Cagliero, D.; Musso, S.; Pavese, M. Oxidation of Carbon Nanotubes for Improving the Mechanical and Electrical Properties of Oil-Well Cement-Based Composites. *ACS Appl. Nano Mater.* **2022**, *5*, 6671.
(21) Tagliaferro, A.; Rovere, M.; Padovano, E.; Bartoli, M.; Giorcelli, M. Introducing the Novel Mixed Gaussian-Lorentzian Lineshape in the Analysis of the Raman Signal of Biochar. *Nanomaterials* **2020**, *10*, 1748.
(22) Budrugeac, P.; Segal, E. Applicability of the Kissinger Equation in Thermal Analysis. *J. Therm. Anal. Calorim.* **2007**, *88*, 703−707.
(23) Orlando, A.; Franceschini, F.; Muscas, C.; Pidkova, S.; Bartoli, M.; Rovere, M.; Tagliaferro, A. A Comprehensive Review on Raman Spectroscopy Applications. *Chemosensors* **2021**, *9*, 262.
(24) Ferrari, A. C.; Robertson, J. Interpretation of Raman Spectra of Disordered and Amorphous Carbon. *Phys. Rev. B: Condens. Matter Mater. Phys.* **2000**, *61*, 14095.
(25) Titus, E.; Ali, N.; Cabral, G.; Gracio, J.; Babu, P.; Jackson, M. Chemically Functionalized Carbon Nanotubes and Their Characterization Using Thermogravimetric Analysis, Fourier Transform Infrared, and Raman Spectroscopy. *J. Mater. Eng. Perform.* **2006**, *15*, 182−186.
(26) Gerry, M.; Lewis-Bevan, W.; Merer, A.; Westwood, N. The infrared spectrum of gaseous aminoborane, H2N═BH2: Location of the fundamentals and rotational structure in the 401 band (BN stretching vibration at 1337 cm−1). *J. Mol. Spectrosc.* **1985**, *110*, 153−163.
(27) Kissinger, H. E. Reaction Kinetics in Differential Thermal Analysis. *Anal. Chem.* **1957**, *29*, 1702−1706.
(28) Gutowska, A.; Li, L.; Shin, Y.; Wang, C. M.; Li, X. S.; Linehan, J. C.; Smith, R. S.; Kay, B. D.; Schmid, B.; Shaw, W.; Gutowski, M.; Autrey, T. Nanoscaffold Mediates Hydrogen Release and the Reactivity of Ammonia Borane. *Angew. Chem.* **2005**, *117*, 3644−3648.
(29) Rassat, S. D.; Aardahl, C. L.; Autrey, T.; Smith, R. S. Thermal Stability of Ammonia Borane: A Case Study for Exothermic Hydrogen Storage Materials. *Energy Fuels* **2010**, *24*, 2596−2606.
(30) Frueh, S.; Kellett, R.; Mallery, C.; Molter, T.; Willis, W. S.; King'ondu, C.; Suib, S. L. Pyrolytic Decomposition of Ammonia Borane to Boron Nitride. *Inorg. Chem.* **2011**, *50*, 783−792.
(31) Nakagawa, T.; Burrell, A. K.; Del Sesto, R. E.; Janicke, M. T.; Nekimken, A. L.; Purdy, G. M.; Paik, B.; Zhong, R.-Q.; Semelsberger, T. A.; Davis, B. L. Physical, Structural, and Dehydrogenation Properties of Ammonia Borane in Ionic Liquids. *RSC Adv.* **2014**, *4*, 21681−21687.
(32) Petit, J.-F.; Demirci, U. B. Discrepancy in the Thermal Decomposition/Dehydrogenation of Ammonia Borane Screened By thermogravimetric Analysis. *Int. J. Hydrogen Energy* **2019**, *44*, 14201−14206.
(33) McBride, J.; Nicholls, R. The Vibration-Rotation Spectrum of Ammonia Gas. I. *J. Phys. B: At. Mol. Phys.* **1972**, *5*, 408.
(34) Anderson, W. E.; Barker, E. The Infra-Red Absorption Spectrum of Diborane. *J. Chem. Phys.* **1950**, *18*, 698−705.
(35) Kaldor, A.; Porter, R. F. Matrix Isolation Study of Borazine and Boroxine. Vibrational Analysis. *Inorg. Chem.* **1971**, *10*, 775−785.
(36) Li, L.; Yao, X.; Sun, C.; Du, A.; Cheng, L.; Zhu, Z.; Yu, C.; Zou, J.; Smith, S. C.; Wang, P.; Cheng, H.-M.; Frost, R. L.; Lu, G. Q. Lithium-Catalyzed Dehydrogenation of Ammonia Borane within Mesoporous Carbon Framework for Chemical Hydrogen Storage. *Adv. Funct. Mater.* **2009**, *19*, 265−271.
(37) Li, H.; Li, Y.; Kang, J.; Fan, L.; Yang, Q.; Li, S.; Rahman, A.; Chen, D. Reactivity and mechanisms of hydridic hydrogen of B-H in ammonia borane towards acetic acids: the ammonia B-monoacyloxy boranes. *New J. Chem.* **2021**, *45*, 9904−9911.

https://doi.org/10.1021/acs.jpcc.2c04693
J. Phys. Chem. C 2022, 126, 16587−16594